MECHANICAL PERFORMANCE OF EPOXY ADHESIVE COMPOSITES REINFORCED WITH WASTE TIRE RUBBER AND COCONUT SHELL BIOCHAR

MADASAMY SERMARAJ,[*] KALIMUTHU RAMANATHAN[**] and K. J. NAGARAJAN[***]

[*]*Department of Mechanical Engineering, Thiagarajar College of Engineering, Madurai 625015, Tamil Nadu, India*
[**]*Department of Mechanical Engineering, Alagappa Chettiar Government College of Engineering and Technology, Karaikudi 630004, Tamil Nadu, India*
[***]*Tamil Nadu Motor Vehicles Maintenance Department, Velachery, Chennai-60042, Tamil Nadu, India*
✉ *Corresponding author: M. Sermaraj, msjmech@tce.edu*

Received January 4, 2026

The disposal of waste tires and coconut shells poses significant environmental challenges, as both materials are often discarded in landfills, contributing to pollution, habitat destruction, and health hazards. This study investigates the incorporation of waste tire particles and coconut shell biochar into epoxy resin–based hybrid polymer composites using the compression molding technique. Pyrolysis was employed to produce coconut shell biochar at temperatures of 400 °C and 800 °C in order to analyze variations in material characteristics. The composites were prepared with different weight proportions of tire rubber and biochar, and properties such as tensile strength, impact strength, and fracture toughness were evaluated. The addition of particles at all concentrations led to significant reduction in impact strength and fracture toughness of the composites compared to the neat resin sample; however, the addition of biochar, particularly at lower to moderate loadings, substantially enhanced tensile strength, with a maximum improvement of 66.1% observed for composites containing biochar produced at 400 °C. The distribution and interfacial adhesion of particles within the resin matrix along the fractured surfaces were examined using scanning electron microscopy, and the nature of failure was identified through morphological analysis. By utilizing waste tire particles and coconut shell biochar, this study aimed to develop materials that are not only mechanically robust, but also contribute to a cleaner and more sustainable future.

Keywords: waste tire rubber, coconut shell biochar, tensile strength, impact strength, fracture toughness

INTRODUCTION

In the dynamic intersection of materials science and environmental sustainability, the reimagining of waste as a valuable resource represents a pivotal avenue for innovation. The disposal of waste tires has emerged as a significant environmental concern, attracting increasing attention due to its severe ecological impacts. Improperly discarded tires contribute to soil and water pollution through the release of harmful chemicals and toxins,[1,2] while their slow decomposition in landfills poses long-term threats to both terrestrial and aquatic ecosystems.[3] Additionally, the combustion of tires releases noxious fumes, exacerbating air pollution.[4,5,6] According to recent studies, India accounts for approximately 6% of the global annual production of 1.6 billion discarded tires,[7] being also the country that imports nearly 300.000 tons of tires annually for recycling purposes. In this context, hybrid composites, formed by combining diverse materials to achieve superior mechanical properties, have emerged as a promising solution across multiple industries.[8,9] Hybrid polymer composites represent a cutting-edge approach to materials engineering by integrating the unique characteristics of different constituents to enhance overall performance.[10] This study focuses on the incorporation of waste materials, specifically discarded tires and coconut shells, into polymer composites, aiming not only to repurpose waste, but also to contribute to the development of sustainable material alternatives.

By strategically blending waste tire particles, coconut shell–derived biochar, and epoxy resin, this work seeks to exploit the synergistic interactions among these components. Waste tire particles are known for their high strength, flexibility, and elasticity,[11] however, their incorporation in materials such as concrete has been shown to reduce overall strength due to the inherent flexibility of rubber, which can compromise structural integrity.[12-13] The production of waste tire particles involves shredding or grinding discarded tires into smaller sizes, followed by the removal of metallic components.[14-15] Advanced processing techniques, including mechanical and cryogenic grinding, enable the production of finer particles, while emerging technologies such as water jet pulverization and supercritical fluid treatment are being explored to further refine material properties.[16]

Biochar, a carbon-rich material produced through the pyrolysis of biomass in an oxygen-limited environment, exhibits desirable characteristics, such as high porosity, basic pH, elevated carbon content, favorable strength-to-weight ratio, and chemical stability.[17-18] Previous studies have demonstrated that the incorporation of biochar into cementitious and polymer matrices can enhance mechanical properties, including flexural strength, fracture energy, and toughness.[19-22] The properties of biochar are influenced by factors such as feedstock type, pyrolysis conditions, temperature, and lignin content.[23] Furthermore, owing to its high surface area, adsorption capacity, ion exchange properties, and porous structure, biochar has also been widely investigated for environmental applications, such as pollutant removal from soil and water systems.[24,25,26]

Epoxy resin is widely recognized for its excellent adhesion, low curing shrinkage, high mechanical strength, and superior electrical insulation properties, making it suitable for a broad range of engineering applications.[27] However, incorporating waste rubber into epoxy-based composites presents challenges because of the high flexibility of rubber, which can adversely affect the strength and mechanical integrity of the resulting material.[28] To overcome this limitation, biochar is introduced as a reinforcing additive, with the expectation that it will enhance the stiffness and overall mechanical performance of the composite.

Based on these considerations, the present study adopted the following methodology. Initially, pyrolysis was employed to produce coconut shell biochar at temperatures of 400 °C and 800 °C. Subsequently, epoxy composites were fabricated by incorporating waste tire particles and coconut shell biochar using a hot-press compression molding technique, with the content of tire particles and biochar as key variables. The mechanical properties of both pure epoxy and the developed composites were evaluated through tensile, impact, and fracture toughness tests. Furthermore, the microstructure of the fractured composite specimens was examined using scanning electron microscopy. This work contributes to a better understanding of the mechanical properties of incorporating waste tire particles and coconut shell biochar –filled epoxy adhesive composites.

EXPERIMENTAL

Materials

Coconut shells were collected from a local coconut market in Coimbatore district, Tamil Nadu, India, while used tires in worn condition were collected from an automobile workshop in Madurai district, Tamil Nadu, India. Diglycidyl ether of bisphenol A (DGEBA)–based epoxy (LY5556), with the density of 0.00112–0.0012 g/mm³, aliphatic amine hardener (HY951), and silicone spray were procured from Parasanna Chemicals, Madurai, Tamil Nadu, India.

Bio-char preparation

The biochar preparation process began by breaking coconut shells into small, manageable pieces, which were then accurately weighed to ensure precision in subsequent steps. The crushed coconut shells were washed with distilled water to remove adhering dust and subsequently dried at 110 °C for 2–3 hours. The dried and weighed coconut shell pieces were then placed in a muffle furnace and carbonized at 200 °C. Following carbonization, the material was ground into smaller particles using a mortar and pestle. Pyrolysis, a process in which biomass is heated under anoxic conditions, was employed to produce biochar; this process may also generate liquid and gaseous by-products while preventing combustion due to the absence of oxygen. The ground carbonized coconut shells were placed inside a cylindrical porcelain crucible (80 mm in diameter and 100 mm in height) and subjected to further heat treatment in an electric muffle furnace.[29] The crucible was covered with a perforated lid to allow the escape of gases and vapors. A temperature of 400 °C was maintained for 180 minutes, after which the furnace was switched off and allowed to cool for approximately 30 minutes before the samples were transferred to a desiccator for further cooling.

The resulting biochar powder, which exhibited a non-uniform particle size distribution, was stored in a desiccator to prevent agglomeration. Subsequently, the biochar was milled using a planetary ball mill for durations up to 240 minutes, resulting in finer particles.

For comparison, the same procedure was repeated at an elevated pyrolysis temperature of 800 °C to investigate the effect of temperature on the characteristics of the biochar.

Rubber particle preparation

Used and discarded rubber tires, collected from various automobile workshops, underwent a systematic deconstruction process, in which the embedded steel wires were carefully removed. The deconstructed tires were then shredded and pulverized to obtain micro-sized rubber particles with a mesh size of 40 (~425 µm).

Preparation of composite material

The preparation of hybrid composites was carried out in accordance with ASTM D638, ASTM D256, and ASTM 5045 standards for tensile, impact, and fracture toughness testing, respectively. Molds were designed using CorelDRAW software and fabricated from acrylic sheets using a CNC laser cutting machine to ensure dimensional accuracy and consistency. Specimens were prepared by mixing epoxy resin with biochar and tire particles in varying weight percentages, as specified in Table 1, followed by the addition of the hardener in a stoichiometric ratio of 10:1 (epoxy:hardener).

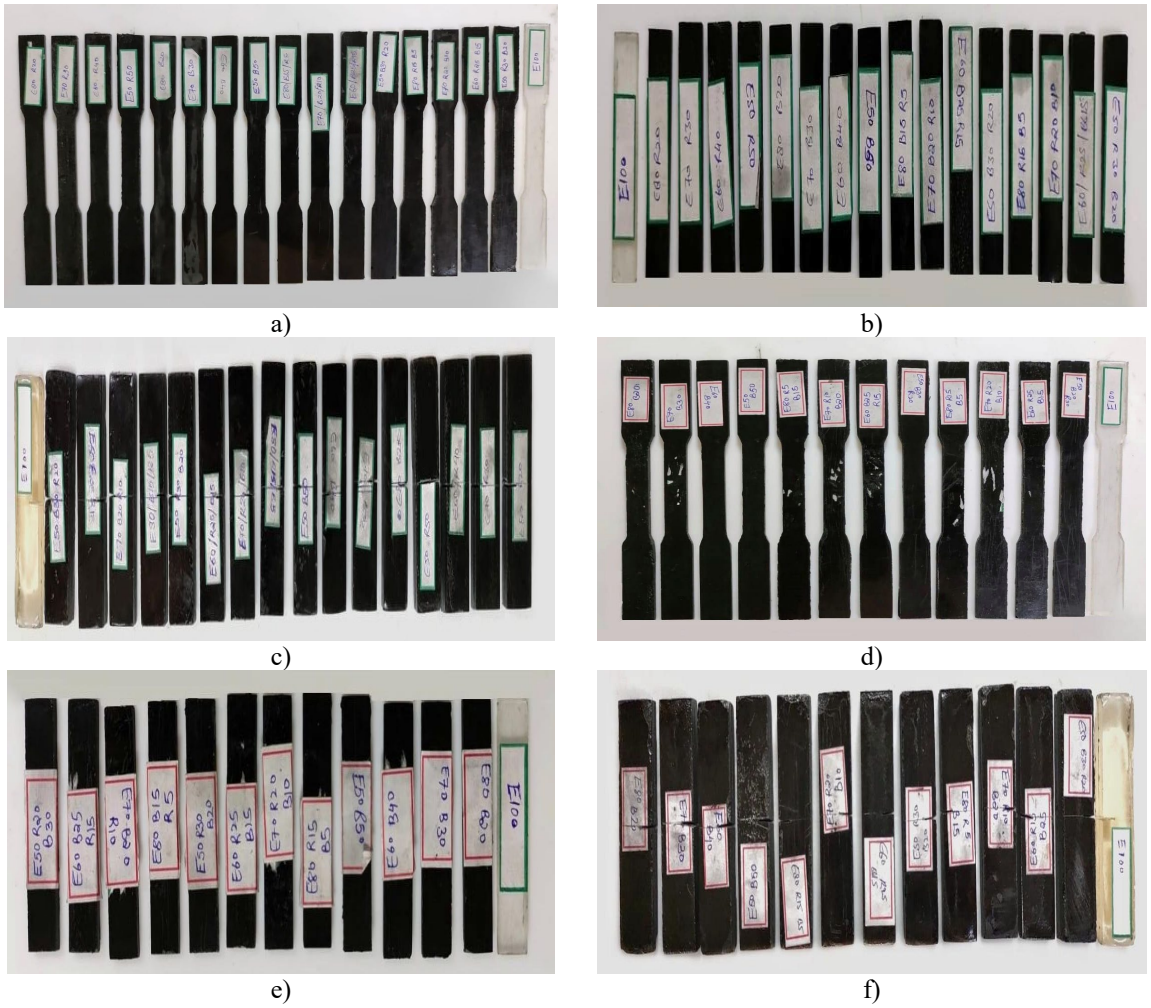

Figure 1: Samples prepared using 400 °C biochar for (a) tensile test, (b) impact test, (c) fracture toughness test; using 800 °C biochar for (d) tensile test, (e) impact test, and (f) fracture toughness test

Prior to casting, a thin layer of petroleum jelly was applied to the mold surfaces to facilitate easy removal of the cured samples. The mixture was thoroughly blended to ensure uniform dispersion of fillers, then carefully poured into the molds and evenly distributed using a spatula to minimize air entrapment.

The molds were subsequently subjected to compression at a pressure of 17 MPa and a processing

temperature of 80 °C for 24 hours. After curing, the specimens were carefully demolded to prevent damage. This procedure was repeated for all compositions while maintaining consistent weight proportions. The prepared specimens, along with neat epoxy for comparison, are presented in Figure 1. For fracture toughness testing, single-edge notched bend (SENB) specimens were prepared in accordance with ASTM 5045-99; notches were introduced using a hacksaw blade, and pre-cracks were initiated at the notch tip using a sharp blade.

Table 1
Formulations and designation of composites

SNo.	Sample	Epoxy (wt%)	Rubber (wt%)	Biochar (wt%)
1.	E100	100	-	-
2.	E80B20	80	-	20
3.	E70B30	70	-	30
4.	E60B40	60	-	40
5.	E50B50	50	-	50
6.	E80R20	80	20	-
7.	E70R30	70	30	-
8.	E60R40	60	40	-
9.	E50R50	50	50	-
10.	E80R15B5	80	15	5
11.	E70R20B10	70	20	10
12.	E60R25B15	60	25	15
13.	E50R30B20	50	30	20
14.	E80R5B15	80	5	15
15.	E70R10B20	70	10	20
16.	E60R15B25	60	15	25
17.	E50R20B30	50	20	30

Mechanical testing

The tensile properties of the composite specimens were evaluated using a universal testing machine (Tinius Olsen H50K). The tests were conducted in accordance with ASTM D638-10 standards using specimens of dimensions 165 mm × 10 mm × 3 mm, at a crosshead speed of 1 mm/min. Fracture toughness was subsequently assessed through a three-point bending test using the same machine at a crosshead speed of 3 mm/min, in accordance with ASTM 5045-99 standards. Impact resistance was evaluated using a Tinius Olsen digital impact testing machine, with a maximum energy capacity of 13.237 J, in accordance with ASTM D256 standards for specimen preparation. All tests were performed five times, and the average values were used for further analysis. The composition of the prepared test specimens, including the weight percentages (wt%) of reinforcement and matrix, is presented in Table 1.

RESULTS AND DISCUSSION

Particle size of biochar produced at 400 °C and 800 °C

Based on the particle size analysis results presented in Figure 2(a) for the biochar sample produced at 400 °C, the differential intensity distribution exhibits a distinct peak around 800 nm, indicating that a significant proportion of particles are concentrated within this size range. The cumulative intensity distribution shows that 50% of the particles have a diameter of 807.9 nm or less, representing the median particle size (D50). This indicates that the particle population is predominantly within the submicron range.

In contrast, the particle size analysis results for the biochar sample produced at 800 °C, as shown in Figure 2 (b), reveal a broader differential intensity peak centred around 950 nm. The cumulative intensity distribution reaches 50% at a particle diameter of 957.3 nm, which is higher than that of the 400 °C sample. This suggests that biochar produced at 800 °C exhibits a relatively coarser particle size distribution. The increase in particle size at higher pyrolysis temperature may be attributed to enhanced particle agglomeration and structural changes during thermal treatment.

Mechanical properties of epoxy and rubber (E+R) composites

The tensile strength and break distance of neat epoxy (E100) were found to be 18.9 MPa and 1.07 mm, respectively, as shown in Figure 3. The tensile properties of epoxy–rubber composites are presented in Figure 4(a). The incorporation of rubber particles (R) into the epoxy matrix

resulted in varying effects on both tensile strength and break distance compared to neat epoxy. The E80R20 composite, containing 20 wt% rubber particles, exhibited a slight increase of 3.2% in tensile strength (19.5 MPa) relative to E100, while the break distance significantly increased by 38.3% to 1.48 mm, indicating enhanced ductility due to rubber reinforcement.[30] However, further increases in rubber content led to a reduction in tensile strength, which can be attributed to weak interfacial adhesion and particle agglomeration. The E70R30 composite showed a 32.8% decrease in tensile strength (12.7 MPa) compared to E100, although the break distance remained higher at 1.44 mm. Similarly, the E60R40 composite exhibited a further decline in tensile strength to 10.1 MPa (a 46.6% reduction), while the break distance increased to 1.97 mm, highlighting a trade-off between strength and ductility. Interestingly, the E50R50 composite, with the highest rubber content (50 wt%), demonstrated a tensile strength of 13.2 MPa (a 30.2% decrease compared to E100), while achieving the maximum break distance of 2.22 mm, indicating significantly improved ductility.[31] Overall, the results show that increasing rubber content enhances elongation and ductility, but at the expense of tensile strength.

Figure 4(b) presents the impact strength values of epoxy and rubber composites. The break energy shows a significant decrease with the incorporation of rubber particles (R) into the epoxy matrix compared to neat epoxy (E100), which exhibits a break energy of 36.17 kJ/m². The E80R20 composite, containing 20 wt% rubber particles, shows a substantial reduction of 92.0%, with a break energy of 8.7 kJ/m². A similar trend is observed for the E60R40 composite, which records a break energy of 8.55 kJ/m², corresponding to a 92.1% decrease relative to E100.

The E70R30 composite exhibits a comparatively higher break energy of 14.05 kJ/m², representing an 87.1% reduction from E100, indicating a slightly improved energy absorption capacity compared to the E80R20 and E60R40 composites.

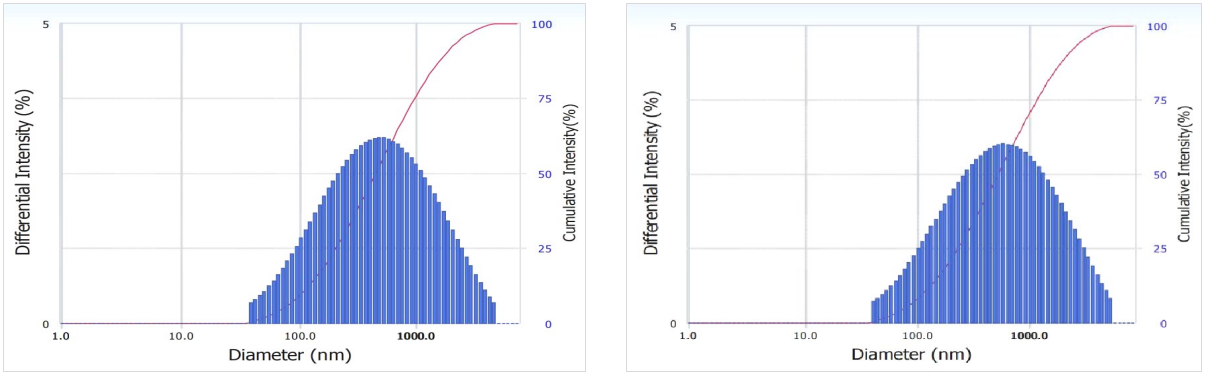

a) b)

Figure 2: Particle size distribution of biochar pyrolyzed at (a) 400 °C, and (b) 800 °C

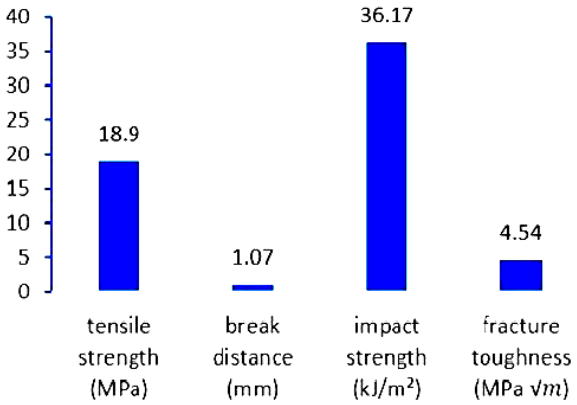

Figure 3: Tensile, break distance, impact strength and fracture toughness of the neat epoxy resin specimen

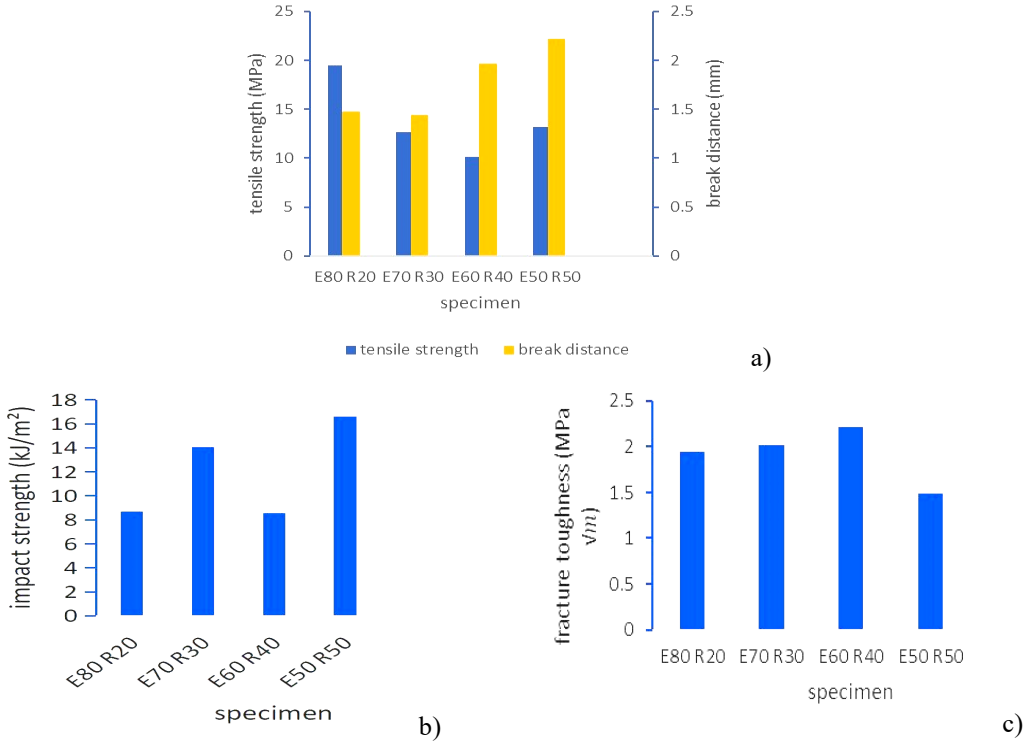

Figure 4: Mechanical properties of E/R composites: (a) tensile strength, (b) impact strength and (c) fracture toughness

The E50R50 composite, with the highest rubber content (50 wt%), demonstrates a break energy of 16.58 kJ/m², corresponding to an 84.7% decrease compared to neat epoxy. Although still lower than E100, this improvement relative to other composites suggests that increasing rubber content enhances impact resistance due to improved energy absorption capability.[32]

Figure 4(c) illustrates the fracture toughness values of epoxy and rubber composites. A notable decrease in fracture toughness is observed with the incorporation of rubber particles compared to neat epoxy (E100), which has a fracture toughness of 4.54 MPa·m$^{1/2}$. This reduction can be attributed to the rubber particles acting as stress concentrators within the epoxy matrix, thereby facilitating crack initiation and propagation.[33] The E80R20 composite exhibits a fracture toughness of 1.94 MPa·m$^{1/2}$, representing a 57.4% reduction compared to E100. Similarly, the E70R30 composite shows a value of 2.02 MPa·m$^{1/2}$, corresponding to a 55.6% decrease. The E60R40 composite demonstrates a slightly higher fracture toughness of 2.21 MPa·m$^{1/2}$, which is 51.3% lower than E100, but higher than that of the E80R20 and E70R30 composites. However, the E50R50 composite, containing the highest rubber content, records the lowest fracture toughness of 1.4 MPa·m$^{1/2}$, indicating a 67.2% reduction compared to neat epoxy.

Mechanical properties of epoxy and 400 °C biochar (E+B) composites

Figure 5(a) presents the tensile properties of epoxy–biochar composites. The incorporation of biochar (B) into the epoxy matrix results in varying effects on tensile strength and break distance compared to neat epoxy (E100). The E80B20 composite, containing 20 wt% biochar, exhibits a significant increase of 66.1% in tensile strength, reaching 31.4 MPa, along with a 71.0% improvement in break distance to 1.83 mm. This simultaneous enhancement in strength and ductility indicates effective load transfer and strong interfacial interaction between the biochar and epoxy matrix. However, increasing the biochar content to 30 wt% (E70B30) leads to a sharp decline in tensile strength to 12.2 MPa (a 35.4% reduction compared to E100), accompanied by a decrease in break distance to 0.72 mm, indicating reduced ductility. The E60B40 composite shows recovery in tensile strength to 26.1 MPa (38.1% higher than E100), with an improved break distance of 1.31 mm, suggesting better stress distribution at this

composition. The E50B50 composite exhibits a tensile strength of 22.0 MPa (16.4% higher than E100), but with a comparatively lower break distance of 1.04 mm than the E80B20 and E60B40 composites.

The impact strength results, shown in Figure 5(c), indicate that the break energy decreases with the addition of biochar compared to neat epoxy, which has a break energy of 36.17 kJ/m². The E80B20 composite shows a 44.4% reduction in break energy to 20.11 kJ/m², while the E70B30 composite records 18.06 kJ/m² (a 50.1% decrease). The E60B40 composite exhibits a further reduction to 15.03 kJ/m² (58.4% decrease). However, the E50B50 composite demonstrates a relatively higher break energy of 23.35 kJ/m² (35.4% reduction), indicating improved energy absorption at higher biochar loading. Overall, the incorporation of biochar reduces impact strength, except at higher loading levels where partial recovery is observed.

Figure 5(e) illustrates the fracture toughness of epoxy–biochar composites. A general decrease in fracture toughness is observed with biochar addition compared to neat epoxy (4.5 MPa·m$^{1/2}$). The E80B20 composite shows a fracture toughness of 2.96 MPa·m$^{1/2}$ (34.9% reduction), while the E70B30 composite further decreases to 2.8 MPa·m$^{1/2}$ (38.4% reduction). This behavior suggests that biochar particles may act as stress concentration sites, promoting crack initiation and propagation. Interestingly, the E60B40 composite exhibits an improved fracture toughness of 3.44 MPa·m$^{1/2}$ (24.4% lower than E100, but higher than E80B20 and E70B30), indicating better resistance to crack growth at this composition. In contrast, the E50B50 composite shows the lowest fracture toughness of 1.99 MPa·m$^{1/2}$ (56.3% reduction), likely due to increased particle agglomeration and reduced matrix continuity at higher filler content.

Mechanical properties of epoxy and 800 °C biochar (E+B) composites

The tensile properties of epoxy composites reinforced with biochar produced at 800 °C are presented in Figure 5(b). The incorporation of high-temperature biochar (B) into the epoxy matrix results in varying effects on tensile strength and break distance compared to neat epoxy (E100), which exhibits a tensile strength of 18.9 MPa and a break distance of 1.07 mm. The E80B20 composite (20 wt% biochar) shows a 30.2% reduction in tensile strength to 13.2 MPa, accompanied by a decrease in break distance to 0.66 mm, indicating a decline in both strength and ductility. The E70B30 composite exhibits a slightly higher tensile strength of 14.4 MPa (23.8% reduction compared to E100), while the break distance further decreases to 0.63 mm, suggesting continued loss of ductility. The E60B40 composite exhibits the highest tensile strength among the 800 °C biochar-reinforced composites, with a value of 15.7 MPa (16.9% lower than E100), along with an improved break distance of 0.91 mm, indicating relatively better stress distribution and energy absorption capacity. The E50B50 composite, with 50 wt% biochar, exhibits the lowest tensile strength of 8.9 MPa (a 52.9% decrease), although the break distance (0.88 mm) is slightly higher than that of lower biochar content composites, suggesting marginal improvement in ductility. Compared to the composites incorporating biochar produced at 400 °C, those with 800 °C biochar demonstrate inferior tensile performance, at optimal filler loadings, which can be attributed to differences in particle size, surface morphology, and the influence of pyrolysis temperature on interfacial bonding characteristics.[29,35]

The impact strength results for 800 °C biochar composites, shown in Figure 5(d), indicate a consistent reduction in break energy compared to neat epoxy (36.17 kJ/m²). The E80B20 composite shows a break energy of 13.91 kJ/m² (61.5% reduction), while the E70B30 composite further decreases to 8.7 kJ/m² (76.0% reduction). The E60B40 composite exhibits the lowest break energy of 8.06 kJ/m² (77.7% reduction), indicating poor energy absorption capability at this composition. The E50B50 composite shows a slight recovery, with a break energy of 9.78 kJ/m² (73.0% reduction). The overall reduction in impact strength with increasing biochar content can be attributed to weak interfacial adhesion and particle agglomeration, which promote crack initiation and brittle failure.

Figure 5(f) illustrates the fracture toughness of epoxy composites reinforced with 800 °C biochar. The neat epoxy exhibits a fracture toughness of 4.5 MPa·m$^{1/2}$, while all composites show reduced values upon biochar addition. The E80B20 composite records a fracture toughness of 1.56 MPa·m$^{1/2}$ (65.5% reduction), whereas the E70B30 composite improves slightly to 1.95 MPa·m$^{1/2}$ (57.1% reduction). The E60B40 composite shows a value of 1.86 MPa·m$^{1/2}$ (59.0% reduction), slightly lower than that of E70B30. Notably, the

E50B50 composite exhibits the highest fracture toughness among the 800 °C biochar composites at 2.96 MPa·m$^{1/2}$, although this still represents a 34.8% reduction compared to neat epoxy. This partial recovery at higher loading may be attributed to increased crack deflection and energy dissipation mechanisms despite the overall reduction in matrix continuity.

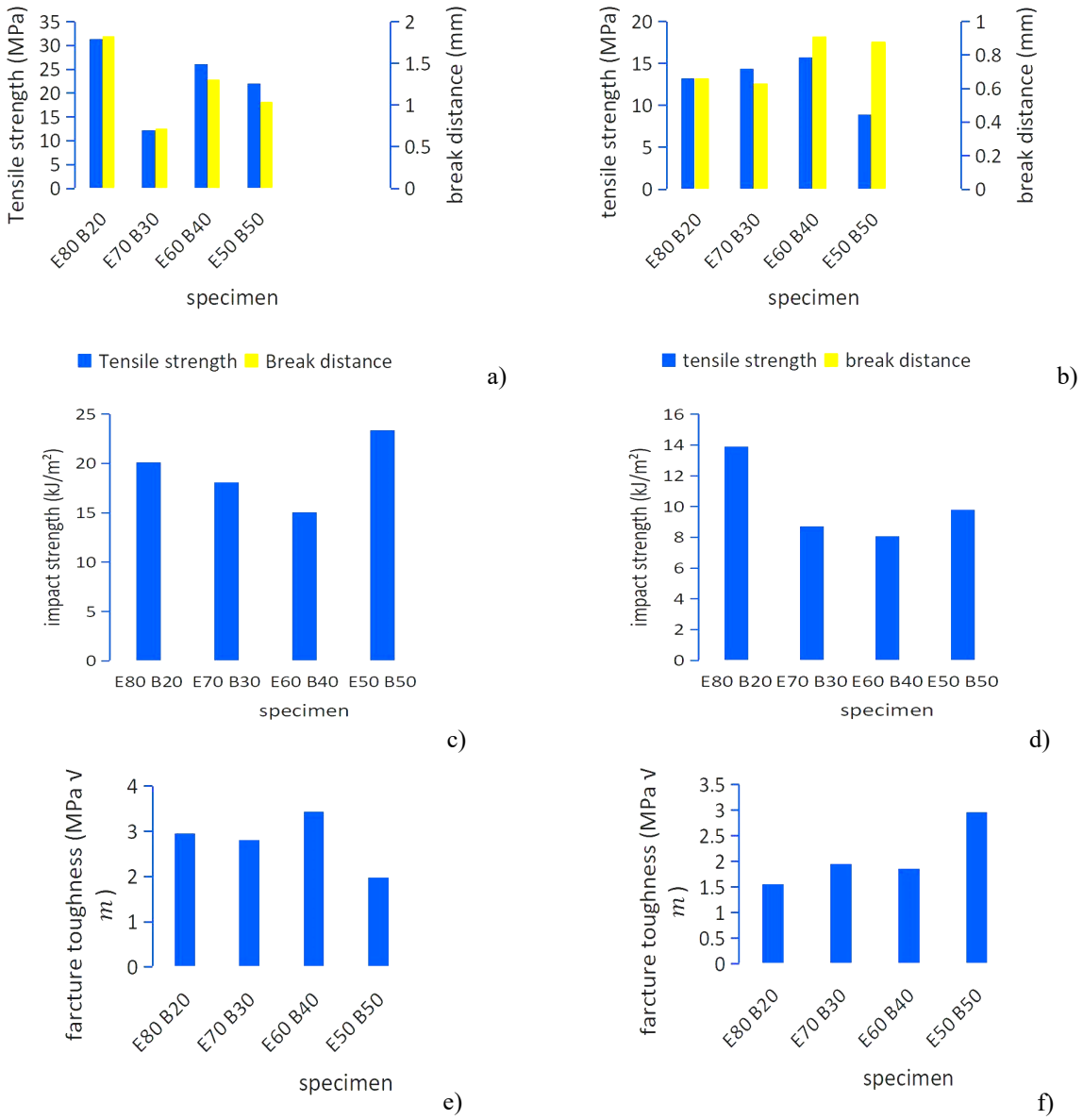

Figure 5: Mechanical properties of E/B composites incorporating 400 °C biochar: a) tensile strength, (c) impact strength, and (e) fracture toughness; Mechanical properties of E/B composites incorporating 800 °C biochar: (b) tensile strength, (d) impact strength, and (f) fracture toughness

Mechanical properties of epoxy, rubber and 400°C biochar composites (E80R15B5, E70R20B10, E60R25B15, E50R30B20)

The incorporation of a combination of rubber particles (R) and biochar (B) into the epoxy matrix results in varying effects on tensile strength and break distance compared to neat epoxy (E100), which exhibits a tensile strength of 18.9 MPa and a break distance of 1.07 mm. The tensile properties are presented in Figure 6(a). The E80R15B5 composite, containing 15 wt% rubber particles and 5 wt% biochar, shows a 22.2% increase in tensile strength to 23.1 MPa, along with a 28.0% increase in break distance to 1.37 mm. This improvement in both strength and ductility indicates a synergistic reinforcement and toughening effect arising from the combined presence of rubber and biochar. The E70R20B10

composite exhibits a tensile strength of 16.5 MPa (12.7% lower than E100), while the break distance remains slightly higher at 1.13 mm. Similarly, the E60R25B15 composite exhibits the same tensile strength (16.5 MPa) as the E70R20B10 composite, but with a higher break distance of 1.47 mm (37.4% higher than E100), indicating enhanced ductility. The E50R30B20 composite, with the highest combined filler content, exhibits the lowest tensile strength of 14.5 MPa (23.3% reduction), while maintaining an improved break distance of 1.39 mm (29.9% increase), further highlighting the trade-off between strength and ductility.

The impact strength results, shown in Figure 6(c), indicate a reduction in break energy for all hybrid composites compared to neat epoxy (36.17 kJ/m²). The E80R15B5 composite records a break energy of 12.05 kJ/m² (66.7% reduction), while the E70R20B10 composite shows a similar value of 12.09 kJ/m² (66.6% reduction). The E60R25B15 composite demonstrates a relatively higher break energy of 14.47 kJ/m² (60.0% reduction), indicating improved energy absorption at this composition. The E50R30B20 composite exhibits a break energy of 12.64 kJ/m² (65.1% reduction), showing slight improvement compared to lower filler combinations.

Figure 6(e) presents the fracture toughness of epoxy–rubber–biochar hybrid composites. A reduction in fracture toughness is observed for all compositions compared to neat epoxy (4.54 $MPa \cdot m^{1/2}$). The E80R15B5 composite exhibits a fracture toughness of 1.78 $MPa \cdot m^{1/2}$ (60.7% reduction), while the E70R20B10 composite shows a slightly higher value of 1.94 $MPa \cdot m^{1/2}$ (57.2% reduction). The E60R25B15 composite records the lowest fracture toughness of 1.46 $MPa \cdot m^{1/2}$ (67.6% reduction), likely due to increased particle interaction and stress concentration effects. The E50R30B20 composite exhibits a fracture toughness of 1.71 $MPa \cdot m^{1/2}$ (62.2% reduction). Overall, the hybrid composites demonstrate improved ductility but reduced fracture resistance, indicating a complex interaction between rubber-induced flexibility and biochar-induced stiffness within the epoxy matrix.

Mechanical properties of epoxy, rubber and 800°C biochar composites (E80R15B5, E70R20B10, E60R25B15, E50R30B20)

The tensile properties of epoxy composites reinforced with a combination of rubber particles (R) and biochar (B) produced at 800 °C are presented in Figure 6(b). The incorporation of these fillers results in varying effects on tensile strength and break distance compared to neat epoxy (E100). The E80R15B5 composite, containing 15 wt% rubber particles and 5 wt% biochar, exhibits a marginal increase in tensile strength to 19.2 MPa, along with a significant improvement in break distance by 54.2% to 1.65 mm, indicating enhanced ductility. The E70R20B10 composite shows a tensile strength of 13.9 MPa (a 26.5% decrease compared to E100), while maintaining a higher break distance of 1.49 mm. The E60R25B15 composite exhibits a further reduction in tensile strength to 11.2 MPa (40.7% decrease), although the break distance increases to 1.24 mm. The E50R30B20 composite, with the highest combined filler content, demonstrates a tensile strength of 14.8 MPa (21.7% reduction), while achieving the highest break distance of 1.85 mm, indicating improved ductility at higher filler loading.

The impact strength results, shown in Figure 6(d), indicate a decrease in break energy for all hybrid composites compared to neat epoxy (E100). The E80R15B5 composite records a break energy of 10.44 kJ/m² (71.1% reduction). The E70R20B10 composite shows an improved value of 12.05 kJ/m² (66.7% reduction), indicating better energy absorption compared to E80R15B5. The E60R25B15 composite exhibits the lowest break energy of 9.09 kJ/m² (74.9% reduction), suggesting reduced resistance to impact loading. Notably, the E50R30B20 composite demonstrates the highest break energy among the hybrid composites at 18.06 kJ/m², although this still represents a 50.1% decrease compared to neat epoxy.

Figure 6(f) illustrates the fracture toughness of epoxy–rubber–biochar composites incorporating biochar produced at 800 °C. The neat epoxy exhibits a fracture toughness of 4.5 $MPa \cdot m^{1/2}$, while all hybrid composites show reduced values. The E80R15B5 composite exhibits a fracture toughness of 1.29 $MPa \cdot m^{1/2}$ (71.6% reduction), and the E70R20B10 composite shows a slightly lower value of 1.15 $MPa \cdot m^{1/2}$ (74.7% reduction). The E60R25B15 composite demonstrates an improved fracture toughness of 1.76 $MPa \cdot m^{1/2}$ (61.3% reduction), indicating better crack resistance compared to lower filler combinations. The E50R30B20 composite exhibits the highest fracture toughness among the hybrid composites at 1.86 $MPa \cdot m^{1/2}$, although this still represents a 59.1% reduction relative to neat epoxy. Overall,

the hybrid composites produced with 800 °C biochar exhibit enhanced ductility, but reduced strength and fracture resistance, highlighting the influence of high-temperature biochar on interfacial bonding and composite performance.

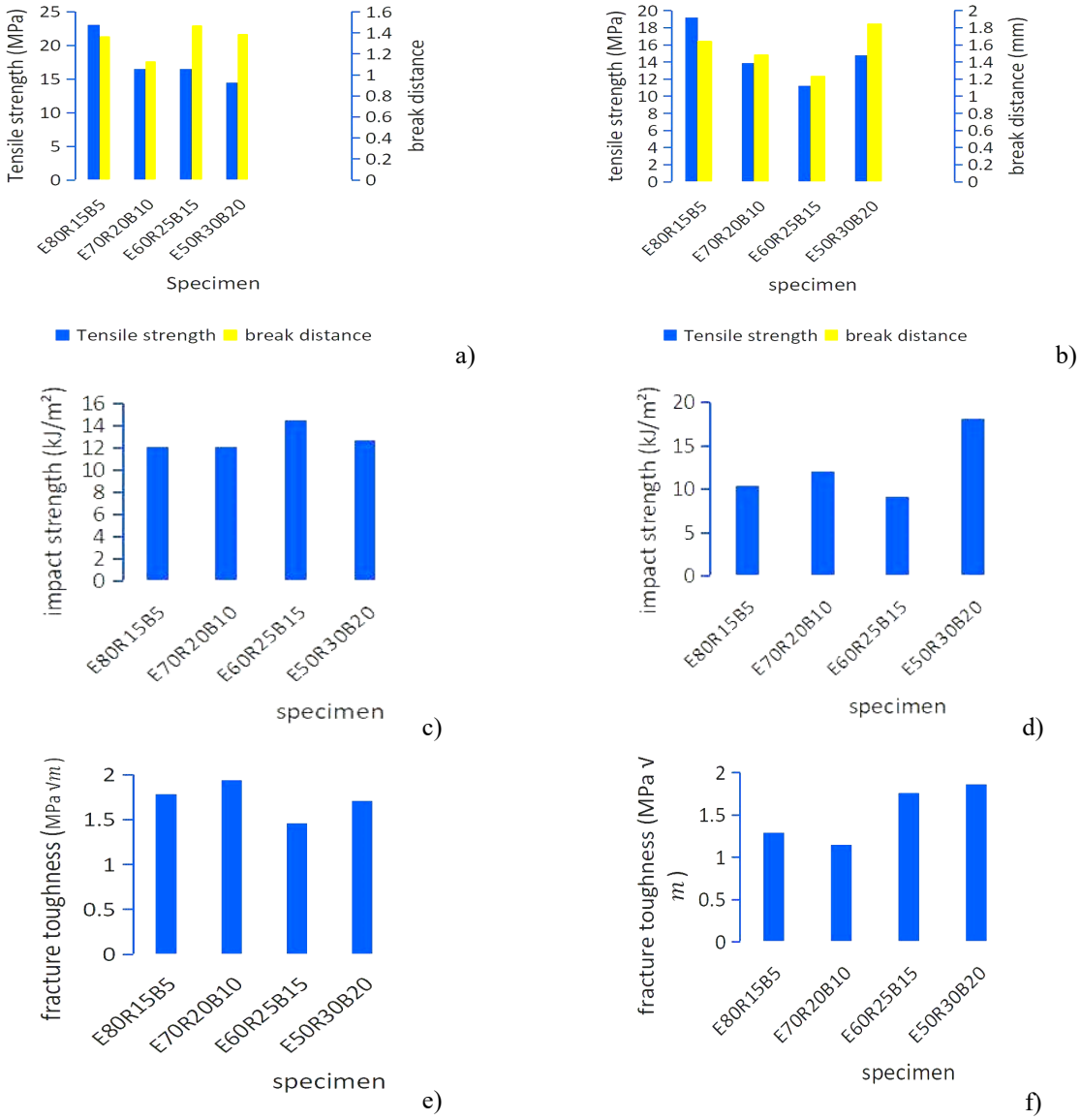

Figure 6: Mechanical properties of E/R/B composites with 400 °C biochar: (a) tensile strength, (c) impact strength, and (e) fracture toughness; E/R/B composites with 800 °C biochar: (b) tensile strength, (d) impact strength, and (f) fracture toughness

Mechanical properties of epoxy, 400 °C biochar and rubber composites (E80R5B15, E70R10B20, E60R15B25, E50R20B30)

The tensile properties of epoxy composites reinforced with biochar and rubber are presented in Figure 7(a). The E80R5B15 composite, containing 5 wt% rubber particles and 15 wt% biochar, exhibits a 12.7% increase in tensile strength (21.3 MPa) along with a 41.1% improvement in break distance (1.51 mm), indicating enhanced strength and ductility due to the combined reinforcing and toughening effects of rubber and biochar. However, the E70R10B20 composite shows a significant reduction in tensile strength to 9.74 MPa (48.5% decrease compared to E100), accompanied by a sharp decrease in break distance to 0.48 mm, indicating brittle behavior. The E60R15B25 composite demonstrates a tensile strength of 12.9 MPa (31.7% reduction), with a slightly higher break distance of 1.12 mm compared to neat epoxy, suggesting limited improvement in ductility. The E50R20B30 composite exhibits the lowest tensile strength of 8.61 MPa (54.4% reduction), along

with a reduced break distance of 0.56 mm, indicating poor mechanical performance at higher filler content.

The impact strength results, shown in Figure 7(c), indicate a substantial decrease in break energy for all hybrid composites compared to neat epoxy (36.17 kJ/m²). The E80R5B15 composite records a break energy of 13.23 kJ/m² (63.4% reduction), while the E70R10B20 composite shows a further decrease to 8.74 kJ/m² (75.8% reduction). The E60R15B25 composite exhibits a break energy of 9.48 kJ/m² (73.8% reduction), slightly higher than that of E70R10B20. The E50R20B30 composite records a break energy of 8.79 kJ/m² (75.7% reduction), indicating consistently low impact resistance at higher filler loadings.

Figure 7(e) presents the fracture toughness values of the composites. The E80R5B15 composite exhibits a fracture toughness of 1.98 $MPa \cdot m^{1/2}$ (56.3% reduction), while the E70R10B20 composite shows a similar value of 1.95 $MPa \cdot m^{1/2}$ (57.0% reduction). The E60R15B25 composite demonstrates a fracture toughness of 1.8 $MPa \cdot m^{1/2}$ (58.6% reduction), and the E50R20B30 composite exhibits a comparable value of 1.8 $MPa \cdot m^{1/2}$ (58.7% reduction). The overall decrease in fracture toughness with increasing filler content indicates weak interfacial bonding and increased stress concentration within the epoxy matrix, which promotes crack initiation and propagation.

Mechanical properties of epoxy, 800 °C biochar and rubber (E80R5B15, E70R10B20, E60R15B25, E50R20B30)

The tensile properties of epoxy composites reinforced with rubber particles (R) and biochar (B) produced at 800 °C are presented in Figure 7(b). The E80R5B15 composite, containing 5 wt% rubber particles and 15 wt% biochar, exhibits a marginal increase in tensile strength to 19.9 MPa (5.3% higher than E100), while the break distance increases slightly to 1.08 mm, indicating limited improvement in ductility. The E70R10B20 composite shows a tensile strength of 18.1 MPa (4.2% lower than E100), with an unchanged break distance of 1.07 mm, suggesting negligible variation in ductility. The E60R15B25 composite exhibits a tensile strength of 18.3 MPa (3.2% lower than E100), accompanied by a slight increase in break distance to 1.13 mm. In contrast, the E50R20B30 composite demonstrates a significant reduction in tensile strength to 7.3 MPa (61.4% lower than E100), while the break distance increases markedly to 1.91 mm (78.5% higher than E100), indicating enhanced ductility at the expense of strength.

The impact strength results, shown in Figure 7(d), exhibit varying trends with biochar produced at 800 °C. The E80R5B15 composite records a break energy of 9.0 kJ/m² (75.1% reduction compared to E100). The E70R10B20 composite shows improved impact performance with a break energy of 14.28 kJ/m² (60.5% reduction). The E60R15B25 composite exhibits a break energy of 10.84 kJ/m² (70.0% reduction), while the E50R20B30 composite shows 12.36 kJ/m² (65.8% reduction). Although all values remain lower than that of neat epoxy, moderate filler combinations demonstrate relatively better energy absorption.

Figure 7(f) presents the fracture toughness of these composites. The E80R5B15 composite exhibits a fracture toughness of 2.22 $MPa \cdot m^{1/2}$ (51.2% reduction), while the E70R10B20 composite shows a lower value of 1.81 $MPa \cdot m^{1/2}$ (60.2% reduction). The E60R15B25 composite demonstrates a fracture toughness of 1.95 $MPa \cdot m^{1/2}$ (57.1% reduction), indicating slight improvement compared to E70R10B20. The E50R20B30 composite exhibits the lowest fracture toughness of 1.67 $MPa \cdot m^{1/2}$ (63.3% reduction). Overall, the results indicate that the incorporation of high-temperature biochar and rubber leads to improved ductility in certain compositions, but reduces strength and fracture resistance due to weak interfacial bonding and increased stress concentration effects.

Morphological study

The morphological characteristics of the fractured surfaces of mechanically tested composite specimens were examined using a VEGA3 SBH scanning electron microscope (TESCAN). This analysis focused on particle distribution and crack propagation behavior on the fractured surfaces. Specimens exhibiting relatively higher tensile strength, impact strength, and fracture toughness were selected from each composition for detailed morphological evaluation. Initially, the fractured regions were cut into 10 × 10 mm squares and then coated with a layer of gold to enhance their conductivity.[36-38]

Figure 8 presents SEM images of the composites at various magnifications. Figure 8(a) shows the morphology of the E60B40 composite (with biochar prepared at 400 °C) at 500×

magnification. The fracture toughness-tested specimen exhibits significant agglomeration of biochar particles, forming large clusters dispersed within the epoxy matrix. Voids and porosity are also evident, likely resulting from poor dispersion or air entrapment during fabrication. The rough and irregular fracture surface indicates a ductile failure mechanism involving particle debonding and matrix tearing.[39]

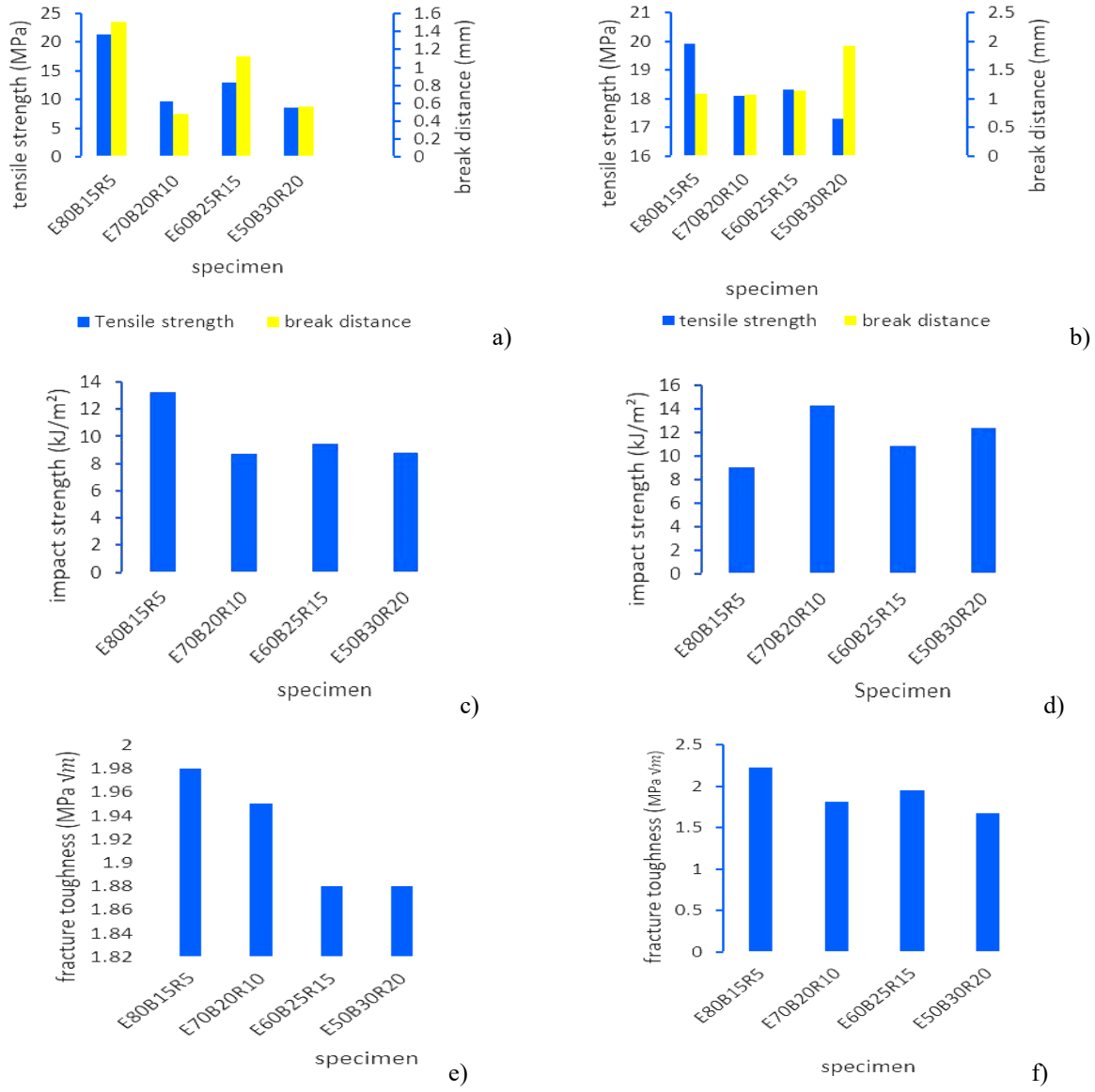

Figure 7: Mechanical properties of E/B/R composites with 400 °C biochar: (a) tensile strength, (c) impact strength, and (e) fracture toughness; E/B/R composites with 800 °C biochar: (b) tensile strength, (d) impact strength, and (f) fracture toughness

Figure 8(b) presents the morphology of the E80R5B15 composite (with biochar prepared at 800 °C) at 91× magnification. The tensile-tested specimen exhibits relatively smaller biochar clusters, indicating reduced agglomeration and fewer visible voids compared to the previous sample, which suggests improved particle dispersion and enhanced interfacial characteristics within the matrix.

Figure 8(c) illustrates the morphology of the E80R15B5 composite (with biochar prepared at 400 °C) at 96× magnification. The SEM image reveals particle agglomeration along with visible voids and pores, indicating non-uniform dispersion and possible weak interfacial bonding.

Figure 8(d) shows the morphology of the E50R30B20 composite (with biochar prepared at 800 °C) at 128× magnification. The impact-tested

specimen exhibits a rough and irregular fracture surface, characteristic of brittle fracture behavior.

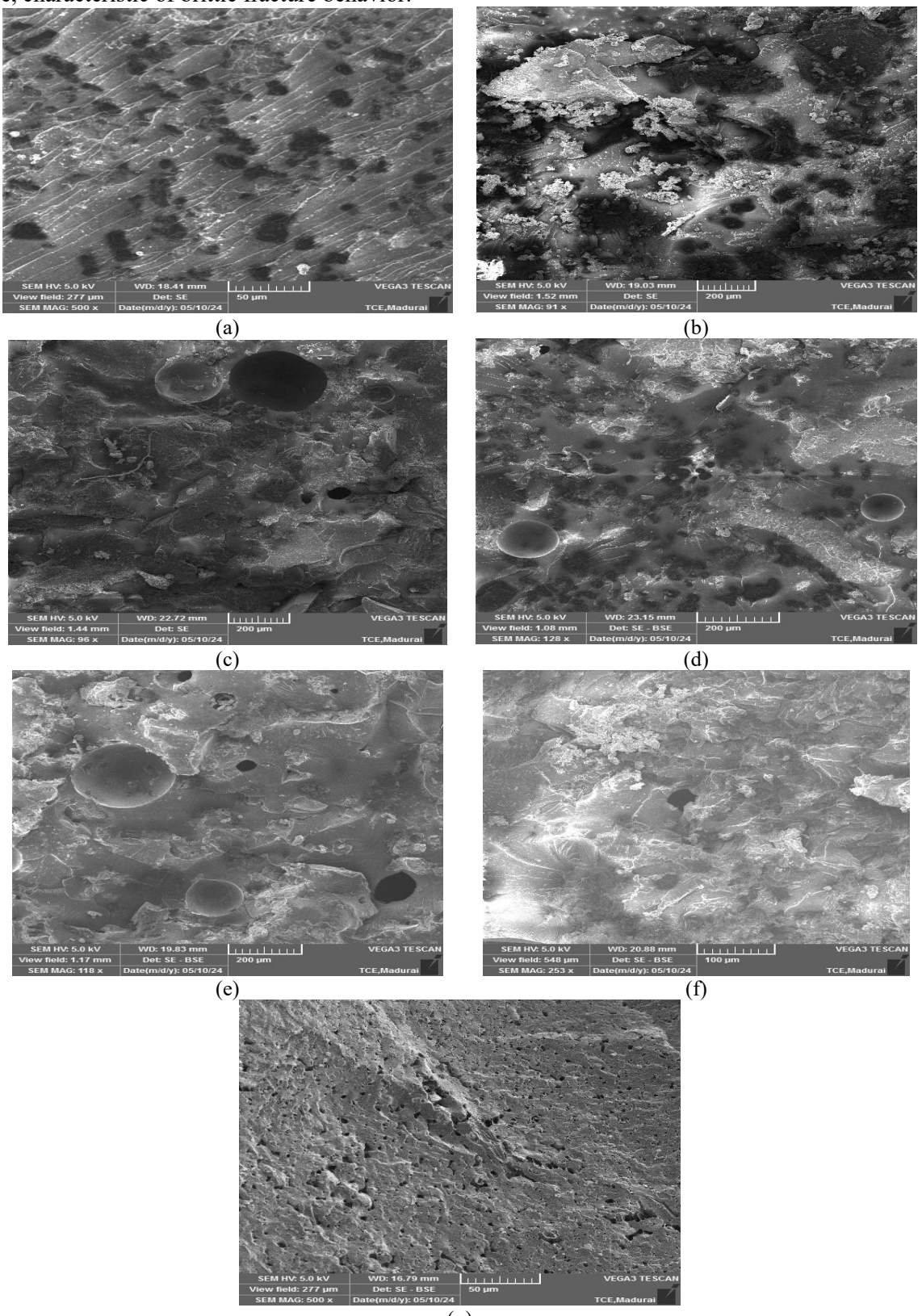

Figure 8: SEM images of fractured surfaces of composites: (a) E80B20 (400 °C), (b) E80R5B15 (800 °C), (c) E80R15B5 (400 °C), (d) E50R30B20 (800 °C), (e) E50R50, (f) E50B50 (800 °C), (g) E80R5B15 (400 °C)

The presence of voids, cavities, and darker regions suggests filler agglomeration and possible debonding between the matrix and reinforcement phases.

Figure 8(e) presents the morphology of the E50R50 composite at 118× magnification. The SEM image reveals a large void or defect within the material, which can act as a stress concentrator and significantly reduce the mechanical strength of the composite.[40]

Figure 8(f) shows the morphology of the E50B50 composite (incorporating biochar prepared at 800 °C) at 253× magnification. The fracture toughness-tested specimen exhibits a relatively rough fracture surface, indicating a more ductile failure mode. The surface appears fairly uniform, with no large agglomerates; however, smaller clusters and closely packed filler regions are visible, contributing to the observed texture.

Figure 8(g) illustrates the morphology of the E80R5B15 composite (with biochar at 400 °C) at 500× magnification. The tensile-tested specimen shows a rough fractured surface with the presence of voids and cavities, indicating defects and weak interfacial adhesion between the filler and matrix phases.

Overall, the SEM analysis reveals that particle agglomeration, void formation, and interfacial bonding significantly influence the mechanical behavior of the composites. Improved dispersion and stronger interfacial adhesion are critical for enhancing composite performance.

CONCLUSION

The composite specimens were successfully fabricated using a compression molding technique with epoxy resin as the matrix and waste rubber particles and coconut shell biochar as reinforcing fillers. The results indicate that the incorporation of these fillers at all concentrations leads to a reduction in impact strength and fracture toughness compared to neat epoxy. However, the addition of lower weight fractions of biochar and rubber particles enhances the tensile strength of the composites. Among the studied compositions, composites reinforced with biochar produced at 400 °C exhibit superior tensile performance compared to those prepared with biochar pyrolyzed at 800 °C, highlighting the significant influence of pyrolysis temperature on the mechanical behavior of the composites.

Furthermore, the inclusion of biochar and rubber particles increases the break distance relative to neat epoxy, indicating improved ductility. The addition of biochar to epoxy–rubber composites also contributes to enhanced impact strength when compared to composites reinforced solely with rubber particles. The comparatively coarser particle size of biochar produced at 800 °C adversely affects the mechanical properties, further emphasizing the role of particle characteristics.

Scanning electron microscopy analysis reveals the presence of particle agglomeration, voids, and cavities within the composite structure, which hinder effective stress transfer between the matrix and reinforcement. These defects can be minimized through improved dispersion techniques and optimized processing conditions. Overall, the utilization of waste tire rubber and coconut shell biochar in composite fabrication offers a sustainable approach to reducing environmental pollution, while enabling the development of cost-effective materials for engineering applications.

REFERENCES

[1] M. Rai, G. Pant, K. Pant, B. N. Aloo, G. Kumar *et al*., *Resources*, **12**, 67 (2023), https://doi.org/10.3390/resources12060067

[2] M. Capolupo, L. Sørensen, K. D. R. Jayasena, A. M. Booth and E. Fabbri, *Water Res*., **169**, 115270 (2020), https://doi.org/10.1016/j.watres.2019.115270

[3] S. Wagner, T. Hüffer, P. Klöckner, M. Wehrhahn, T. Hofmann *et al*., *Water Res*., **139**, 83 (2018), https://doi.org/10.1016/j.watres.2018.03.051

[4] K. Sana, M. Paraschiv, R. Kuncser, M. Tazerout, M. Prisecaru *et al*., *J. Eng. Des. Res*., **20**, 52 (2014), https://doi.org/10.29081/jesr.v20i4.52

[5] D. Mentes, C. E. Tóth, G. Nagy, G. Muránszky and C. Póliska, *Waste Manage*., **149**, 302 (2022), https://doi.org/10.1016/j.wasman.2022.06.028

[6] Y. A. Levendis, A. Atal, J. Carlson, Y. Dunayevskiy and P. Vouros, *Environ. Sci. Technol*., **30**, 2742 (1996), https://doi.org/10.1021/es950948h

[7] P. N. Bansal and D. B. Kapgate, *Int. J. Res. Appl. Sci. Eng. Technol*., **11**, 134 (2023), https://doi.org/10.22214/ijraset.2023.47691

[8] N. M. Nurazzi, M. R. M. Asyraf and S. Fatimah Athiyah, *Polymers*, **13**, 2170 (2021), https://doi.org/10.3390/polym13132170

[9] M. S. El-Wazery, *J. Mater. Environ. Sci*., **8**, 666 (2017)

[10] N. M. Gururaja and A. N. Hari Rao, *Int. J. Soft Comput. Eng*., **1**, 352 (2012), https://www.ijsce.org/portfolio-item/F0342121611/

[11] A. N. Gent and J. D. Walter, *Composites*, **8**, 271 (1977), https://doi.org/10.1016/0010-4361(77)90226-3

[12] A. Siddika, M. A. A. Mamun, R. Alyousef, Y. H. M. Amran, F. Aslani *et al*., *Constr. Build. Mater*., **224**, 711 (2019), https://doi.org/10.1016/j.conbuildmat.2019.07.108

[13] M. Sambucci and M. Valente, *Materials*, **14**, 7493 (2021), https://doi.org/10.3390/ma14247493
[14] J. Adhikari, A. Das, T. Sinha, P. Saha and J. K. Kim, "Rubber Recycling: Challenges and Developments", 2018, https://doi.org/10.1039/9781788012219-00097
[15] A. Fazli and D. Rodrigue, *Polymers*, **14**, 3933 (2022), https://doi.org/10.3390/polym14193933
[16] K. Formela, *Adv. Ind. Eng. Polym. Res.*, **4**, 209 (2021), https://doi.org/10.1016/j.aiepr.2021.06.003
[17] M. Tripathi, J. N. Sahu and P. Ganesan, *Renew. Sustain. Energy Rev.*, **55**, 467 (2016), https://doi.org/10.1016/j.rser.2015.10.122
[18] I. Cosentino, L. Restuccia, G. A. Ferro and J. M. Tulliani, *Theor. Appl. Fract. Mech.*, **103**, 102261 (2019), https://doi.org/10.1016/j.tafmec.2019.102261
[19] A. K. Subhani, M. Nisar and A. Khitab, *Eng. Proc.*, **44**, 7 (2023), https://doi.org/10.3390/engproc2023044007
[20] C. Das, S. Tamrakar, A. Kiziltas and X. Xie, *Polymers*, **13**, 2663 (2021), https://doi.org/10.3390/polym13162663
[21] M. Giorcelli, A. Khan, N. M. Pugno, C. Rosso and A. Tagliaferro, *Biomass Bioenerg.*, **120**, 219 (2019), https://doi.org/10.1016/j.biombioe.2018.11.013
[22] O. P. Minugu, R. Gujjala, O. Shakuntala, P. Manoj and M. S. Chowdary, *Proc. Inst. Mech. Eng. Part C*, **235**, 5626 (2021), https://doi.org/10.1177/09544062211008077
[23] K. Weber and P. Quicker, *Fuel*, **217**, 240 (2018), https://doi.org/10.1016/j.fuel.2017.12.054
[24] Z. Kang, X. Jia and Y. Zhang, *Sustainability*, **14**, 10128 (2022), https://doi.org/10.3390/su141610128
[25] J. Wang and S. Wang, *J. Clean. Prod.*, **227**, 1002 (2019), https://doi.org/10.1016/j.jclepro.2019.04.282
[26] M. Qiu, L. Liu and Q. Ling, *Biochar*, **4**, 19 (2022), https://doi.org/10.1007/s42773-022-00146-w
[27] R. Zhang, *Appl. Comput. Eng.*, **7**, 208 (2023), https://doi.org/10.54254/2755-2721/7/20230467
[28] C. F. Revelo, M. Correa, C. Aguilar and H. A. Colorado, *Case Stud. Constr. Mater.*, **15**, e00681 (2021), https://doi.org/10.1016/j.cscm.2021.e00681
[29] S. Richard, J. S. Rajadurai and V. Manikandan, *Int. J. Polym. Anal. Charact.*, **21**, 462 (2016), https://doi.org/10.1080/1023666X.2016.1179204
[30] X. Colom, J. Cañavate and F. Carrillo, *Eur. Polym. J.*, **42**, 2369 (2006), https://doi.org/10.1016/j.eurpolymj.2006.05.028
[31] R. Faizah, I. Satyarno, H. Priyosulistyo and A. Aminullah, *J. Phys. Sci.*, **29**, 117 (2018), https://doi.org/10.21315/jps2018.29.s2.9
[32] N. Dishovsky, N. Delchev and N. Ivanova, *J. Chem. Technol. Metall.*, **55**, 2061 (2020)
[33] H. R. Karimi, M. R. M. Aliha and P. Ebneabbasi, *Theor. Appl. Fract. Mech.*, **123**, 103722 (2023), https://doi.org/10.1016/j.tafmec.2022.103722
[34] S. Richard, J. S. Rajadurai and V. Manikandan, *Int. J. Polym. Anal. Charact.*, **21**, 462 (2016), https://doi.org/10.1080/1023666X.2016.1179204
[35] A. Y. Elnour, A. A. Alghyamah and H. M. Shaikh, *Appl. Sci.*, **9**, 1149 (2019), https://doi.org/10.3390/app9061149
[36] S. T. K. Rajan, K. J. Nagarajan and V. Balasubramani, *Int. J. Adhes. Adhes.*, **126**, 103492 (2023), https://doi.org/10.1016/j.ijadhadh.2023.103492
[37] G. R. Raghav, R. A. Kumar, N. K. Jawaharlal, C. Vignesh, F. S. Arockiasamy *et al.*, *Cellulose Chem. Technol.*, **57**, 855 (2023), https://doi.org/10.35812/CelluloseChemTechnol.2023.57.75
[38] B. T. Parthasarathi, S. Arunachalam, N. K. Jawaharlal and M. C. R. Balasundaram, *Cellulose Chem. Technol.*, **58**, 349 (2024), https://doi.org/10.35812/CelluloseChemTechnol.2024.58.34
[39] S. Satapathy, A. Nag and G. B. Nando, *Process Saf. Environ. Prot.*, **88**, 131 (2010), https://doi.org/10.1016/j.psep.2009.11.003
[40] Y. Li, Q. Li and H. Ma, *Compos. Part A*, **72**, 40 (2015), https://doi.org/10.1016/j.compositesa.2015.01.021